Research Article

Syed Ali Rizwan*, Muhammad Nasir Amin, Hafiz Sajid Ali, Hamza Ali, Muhammad Tahir Qadir* and Muhammad Imran

Self-compacting mortar overlays using expanded polystyrene beads for thermal performance and energy efficiency in buildings

https://doi.org/10.1515/rams-2025-0178
Received March 6, 2025; accepted October 28, 2025;
published online December 3, 2025

Abstract: This study presents a novel approach for building thermal retrofitting using self-compacting mortar overlays (SCMO) incorporating low-volume expanded polystyrene beads (EPSBs). Unlike previous high-volume EPSBs concrete applications (20–80 % replacement), this research focuses on thin overlay systems using minimal EPSB content (0.1–0.2 % by binder mass) to achieve thermal benefits without structural compromise. 10 SCMO formulations were developed using three EPSBs sizes (3, 6, 9 mm) with Acacia Nilotica gum as a natural viscosity enhancer. Results revealed that all mixtures having polycarboxylate-ether superplasticizer achieved target flow of 30 ± 1 cm using Hagerman's cone of size ($6 \times 7 \times 10$) cm^3. Comprehensive testing revealed that EPSBs incorporation resulted in increased superplasticizer demand (0.75–0.90 %), extended setting times (93–210 min delay), and reduced compressive strength (50.5–21.9 MPa for largest beads of size 9 mm). However, thermal conductivity decreased significantly from 0.1589 W/m·K (control) to 0.0615 W/m·K (9 mm EPSBs), representing 61.3 % reduction. Early shrinkage testing showed beneficial strain accommodation with EPSBs inclusion. The data presented enables the selection of suitable EPSBs size in SCMO of varying selectable thicknesses. Heat transfer analysis demonstrated energy consumption reductions of 36.3 %, 46.8 %, and 61.3 % for 3, 6, and 9 mm EPSBs sizes, respectively, in 38 mm overlay applications. The results establish SCMO as practical solutions for building thermal retrofitting, offering superior applicability compared to rigid insulation boards while maintaining adequate mechanical properties for overlay applications. This research provides the first systematic evaluation of low-volume EPSBs systems specifically designed for thin overlay thermal retrofitting. The strength reduction can be minimized by using synergy of supplementary cementitious materials, as has been demonstrated by authors in previous studies.

Keywords: self-compacting mortar overlays; expanded polystyrene beads; thermal conductivity; shrinkage; energy efficiency

1 Introduction

The global building sector accounts for approximately 38 % of annual energy consumption, with a significant portion dedicated to maintaining indoor thermal comfort [1, 2]. As urbanization accelerates and climate change intensifies temperature extremes, the demand for energy-efficient building materials has become critical [3, 4]. Traditional approaches to building thermal performance improvement include bulk insulation materials, reflective coatings, and phase-change materials, each with specific advantages and limitations [5, 6].

New technologies, such as self-compacting cementitious systems, may be used imaginatively in the form of concrete overlays [7, 8]. Self-compacting cement paste and mortars incorporating expanded polystyrene beads (EPSBs) have been used for this purpose, and many researchers have reported such techniques previously [9]. The use of EPSBs happens to be a good option for manufacturing energy-efficient self-compacting mortar overlays due to their excellent thermal properties, relatively low density, and moisture resistance [10]. The density of EPSBs ranges between 10 and 20 kg/m^3 and it is an environment-friendly

***Corresponding authors: Syed Ali Rizwan**, Department of Civil Engineering, National University of Computer & Emerging Sciences (NUCES-FAST), Lahore, Pakistan, E-mail: syed.ali@nu.edu.pk; and **Muhammad Tahir Qadir**, Department of Civil and Environmental Engineering, College of Engineering, King Faisal University, 31982, Al Ahsa, Saudi Arabia, E-mail: mqdir@kfu.edu.sa
Muhammad Nasir Amin and Muhammad Imran, School of Civil and Environmental Engineering (SCEE), NUST Institute of Civil Engineering (NICE), National University of Sciences and Technology (NUST), Sector H-12, Islamabad, Pakistan. https://orcid.org/0000-0002-3789-2503 (M. Imran)
Hafiz Sajid Ali and Hamza Ali, Department of Civil Engineering, National University of Computer & Emerging Sciences (NUCES-FAST), Lahore, Pakistan

waste product without any adverse effects on the environment [11]. Research has been conducted on the use of EPSBs as aggregate replacement in concrete to study the thermal and mechanical properties of concrete [12].

Herihiri et al. [13] conducted a study to investigate the physical, mechanical, and thermal properties of the mortars by replacing sand with EPSBs in the ratio of 0, 5, 10, 15, 20, 25, and 100 %. They found that using EPSBs decreases mechanical properties but enhances the thermal properties and satisfies the requirements of insulations of buildings. Sabaa and Ravindrarajah [14] showed the effect of replacing coarse aggregate with recycled polystyrene beads and reported that density and compressive strength reduced with an increase in percentage replacement. Shrinkage increased with increasing polystyrene percentage for both low- and high-density mixes. Hilal et al. [15] analyzed six formulations for lightweight self-compacting concrete by using EPSBs and showed an improvement of workability with increasing EPSBs ratio. Although a decrease in compressive strength was observed, however, it is still acceptable as per ACI standards for structural purposes. Another important research on EPSBs concrete with fly ash was conducted by Babu et al. [16] and he observed that flow properties of these mixes were better than normal concrete made up of normal crushed aggregates while strength decreased with increase in EPSBs proportion in the mix.

However, existing research has primarily focused on bulk concrete applications rather than thin overlay systems. These approaches, while effective for new construction, present limitations for retrofitting existing buildings due to structural load implications and application complexity. A critical research gap exists in developing low-volume EPSBs systems specifically designed for thin overlay applications on existing building surfaces. Unlike bulk concrete modifications that require structural considerations, thin overlays (20–50 mm) can provide thermal enhancement without significant load addition or structural modification. Moreover, the research gap can be identified in the sense that such energy-efficient techniques have been rarely reported in the literature and that this study aims at reducing/increasing the internal temperatures in summer and winters, respectively, by modifying the temperature humidity interaction. The challenge lies in achieving meaningful thermal improvement with minimal EPSBs content while maintaining adequate mechanical properties and workability for overlay placement.

Compared to other thermal retrofit strategies, the SCMO developed in this study offers a unique balance of low thermal conductivity (0.0615–0.1589 W/m·K), minimal structural impact, and ease of application. While Hilal et al. [15] utilized EPS content with over 100 mm thickness, their approach demands significant structural support and high installation complexity due to formwork requirements. Aerogel plasters, although exhibiting ultra-low thermal conductivity (0.012–0.025 W/m·K), are constrained by high cost and moderate complexity [17, 18]. EPS foam boards, widely used in practice, require adhesive-based medium-complexity installation and add bulk (50–200 mm), but offer no structural benefit [19, 20]. Phase change materials offer thermal benefits (0.15–0.25 W/m·K) within thinner layers but demand high encapsulation efforts [21, 22]. In contrast, the SCMO method requires only 0.1–0.2 % EPSBs by mass, applies at a thickness of 20–50 mm, and is self-placing, offering excellent adaptability for complex geometries while maintaining minimal installation complexity and structural intrusion.

There has been reported research on incorporating EPSBs in self-compacting concrete. Either they had high EPSBs content or were employed throughout the concrete matrix. This study introduces a novel approach using self-compacting mortar overlays (SCMO) with low-volume EPSBs incorporation (0.1–0.2 % by binder mass) specifically designed for building retrofit applications. The self-compacting property eliminates the need for mechanical vibration during placement, making it particularly suitable for overlay applications on vertical or overhead surfaces. This study provides the following specific contributions: (1) Novel Low-Volume Approach: Development of thermally effective SCMO using significantly lower EPSBs contents (0.1–0.2 %) compared to existing literature (20–80 %), making them suitable for thin overlay applications. (2) Natural Admixture Integration: First systematic study incorporating Acacia Nilotica gum as a natural viscosity-enhancing agent in EPSBs-modified systems, providing sustainable admixture alternatives. (3) Comprehensive Performance Evaluation: Complete characterization including fresh properties, mechanical performance, thermal conductivity, and energy efficiency calculations specifically for overlay applications. (4) Practical Energy Analysis: Quantitative assessment of energy consumption reduction (36.3–61.3 %) using Fourier heat transfer analysis for real-world building conditions. (5) Size Effect Investigation: Systematic evaluation of EPSBs size influence (3, 6, 9 mm) on thermal and mechanical properties for optimal selection in overlay applications.

2 Experimental part

2.1 Materials

Samples were prepared from a mixture of ordinary Portland cement (OPC), EPSBs, polycarboxylate-ether based superplasticizer (SP, Melflux 2651 F), and locally available organic Acacia Nilotica acting as a viscosity-enhancing agent, which

(a) OPC (b) Polystyrene beads (c) Acacia Nilotica gum powder

Figure 1: Materials used in the preparation of self-compacting mortar specimens.

is also a proven useful admixture [23–25]. OPC of Type-1 42.5 R [26] was used. Figure 1 shows the materials used in the formulations. The chemical formula of EPSBs is $(C_8H_8)_n$) which is insoluble in water and soluble in benzene, carbon disulfide, and chloroform. The density, melting point, boiling point, and thermal conductivity of EPSBs were 8–9 kg/m^3, ~ 240 °C, 430 °C, and 0.033 W/(m·K), respectively.

Expanded Polystyrene Beads (EPSBs) used in this study exhibited low densities ranging from 8 to 9 kg/m^3, with internal porosity exceeding 97 % across all sizes. Surface area decreased with increasing bead size, while water absorption remained low (0.09–0.15 %), consistent with their closed-cell structure and hydrophobic nature, confirmed by water contact angles exceeding 90°. Beads were near-spherical with slight shape deviation (aspect ratio 1.1–1.3), and their chemical composition consisted of >98 % pure expanded polystyrene with minimal additives. ANG (Acacia Nilotica Gum) was selected as a multifunctional admixture due to its moderate viscosity-enhancing capability, complete water solubility, and biodegradability. With a molecular weight of 250–580 kDa and thermal stability up to 80 °C, ANG offered suitable performance for SCMO. Compared to commercial VEAs such as welan gum, xanthan gum, and cellulose ethers, ANG demonstrated clear advantages in cost-efficiency ($2.5/kg vs $8–35/kg), environmental sustainability, and regional availability. Its dual function as a viscosity modifier and internal curing agent made it especially suitable for overlays, providing adequate rheological control without compromising strength development.

Compared to conventional viscosity-enhancing agents (VEAs), Acacia Nilotica Gum (ANG) offers a sustainable and cost-effective alternative with a dual mechanism: physical thickening and internal curing [23]. While commercial gums like welan and xanthan function via hydrogen bonding or polymer chain entanglement, they are 6–12 times more expensive and derived from synthetic fermentation. Cellulose ethers involve chemical modification, and clay-based VEAs, though natural, require much higher dosages (up to 2 %). In contrast, ANG operates effectively at a 0.33 % dosage by enhancing viscosity to suspend EPSBs and supplying internal curing through its hygroscopic nature. This is especially beneficial for thin overlays with limited external curing. FTIR analysis confirms that ANG does not chemically react with cementitious phases but interacts physically via hydrogen bonding with pore solution, maintaining hydration compatibility. Its biodegradable and renewable nature further strengthens its environmental appeal, making it a suitable choice for sustainable thermal mortars.

2.2 Mix proportions

In this research, a total of 10 SCMO formulations were studied with a view to finding a better energy-efficient system. The control sample (CS) had cement, sand, and a superplasticizer whereas other samples, i.e., S2 to S10, were prepared using a constant quantity of cement, sand, Acacia Nilotica gum (ANG) powder, and water-to-cement ratio along with varying ratios and sizes of polystyrene beads. The ratio of cement: sand was 1:1 by weight. Generally, the fresh density of SCMO using the stated mix proportions and w/c ratios lies within the range of 2–2.2 g/cm^{3,} which enables the quantities to be worked out for a given volume [25]. For all 10 formulations, the water to cement ratio was 0.4. The water-to-cement ratio of 0.4 was calculated as the mass ratio of mixing water to cement only (not including sand). With cement and sand taken in equal weights (1:1 ratio), the total water-to-binder ratio considering both cement and sand would be 0.2. However, for consistency with standard concrete terminology, the w/c ratio refers specifically to water-to-cement mass ratio. The ANG powder was taken as 0.33 % by weight of cement as recommended [25]. EPSBs and SP ratios were taken in terms of the weight of binder. SP dosage was determined by trials for a target flow of 30 ± 1 cm using Hagerman's mini slump cone [27]. The laboratory temperature and relative humidity were 22 °C and 45 %, respectively, while the mixing water temperature was kept at 22 °C.

The selection of a low EPSBs content range (0.1–0.2 % by binder mass, or 0.038–0.076 % by volume) was strategically made to meet the unique demands of overlay applications. Unlike high-volume EPSBs concretes, which often compromise compressive strength and structural integrity, this low content preserves bond strength and minimizes the risk of delamination or cracking. It also maintains self-compacting

workability – crucial for overlays placed without vibration – as higher EPSBs levels (>0.3 %) were found to hinder flow even with increased superplasticizer dosage. Economically, the approach offers thermal benefits at lower cost and avoids the need for specialized mixing. Given the limited thickness of overlays (20–50 mm), optimizing thermal performance within this constraint is critical. Additionally, the selected content allows practical deployment using conventional tools and methods. Overall, this low-EPSBs strategy shifts the paradigm from bulk insulation to surface-level enhancement, delivering thermal efficiency without compromising structural or functional viability.

2.3 Mixing regime

The dry mixing of EPSBs, cement, sand, ANG powder, and powdered Melflux 2651 F was done for 1 min in the Hobart mixer of 5-L capacity, followed by the addition of 80 % of the total mixing water. The mixing was done for 1 min at a slow rotational speed of 145 rpm. The remaining 20 % of water was added and mixed at a high rotational mixing speed of 285 rpm for 2 min. Mixing procedure as per BS-EN 196–3 [28] and total mixing time was 4 min. The temperature of the mixing water and the lab was maintained at 22–23 °C. Meanwhile, relative humidity was maintained in the range of 40–45 %. After mixing at the fresh state, it is worth mentioning that no signs of bleeding, segregation, or clustering of EPSB was observed.

2.4 Casting of specimens

Prisms of dimensions $(40 \times 40 \times 160)$ mm^3, as prescribed by BS-EN 196–1 [29], were cast. The formulation details are given in Table 1.

Table 1: Description of mixture proportions of different SCMO.

Formulation ID	W/C ratio	Polystyrene beads size (mm)	EPSBs (%)	Melflux 2651 F (%)
CS	0.4	–	–	0.4
S2	0.4	3	0.1	0.75
S3	0.4	3	0.15	0.75
S4	0.4	3	0.2	0.75
S5	0.4	6	0.1	0.85
S6	0.4	6	0.15	0.85
S7	0.4	6	0.2	0.85
S8	0.4	9	0.1	0.9
S9	0.4	9	0.15	0.9
S10	0.4	9	0.2	0.9

After casting, the prisms were then covered with a polythene sheet for an initial 24 h such that the moisture present in the samples was not lost to the environment [30]. After demolding the samples, they were numbered, marked and weighed. Afterwards they were immersed in water at 22 °C in a curing tank until the testing age/(s) in saturated surface-dry (SSD) condition [31].

3 Results and discussion

3.1 X-ray fluorescence test on OPC

The mineralogical composition of OPC was determined by the X-ray fluorescence test as shown in Table 2. Moreover, Table 2 shows the Bogue potential phases of OPC along with other oxides and gypsum modifications.

The chemical composition and Bogue potentials presented in Table 2 are essential for understanding the hydration kinetics and thermal behavior observed in subsequent sections. The high C_3S content (45.62 %) contributes to early strength development, while the C_3A content (8.22 %) influences the effectiveness of the superplasticizer and setting time modifications observed with EPSBs addition.

3.2 Superplasticizer demand of SCMO

For the determination of the SP demand (%) of SCMO, Hagerman's mini slump cone of dimensions $(6 \times 7 \times 10)$ cm^3 was used. Figure 2 shows the results of the SP demand test for the target flow of various formulations using different EPSBs sizes. The test results reported represent average of three tested readings. It should be noted that by increasing ESPBs from 0.1-0.2 % for the same ESPB size 3, 6, or 9 mm), Melflux quantity remains the same because of the flexibility of the target flow (30 ± 1 cm) and internal friction within the matrix and at the interface starts increasing with the increase in size of beads and not with the small percentage difference of EPSBs.

The observed increase in SP demand with EPSBs size (from 0.75 % for 3 mm to 0.90 % for 9 mm beads) can be mechanistically explained through several interrelated factors. First, despite larger beads having a lower specific surface area, the total interfacial area with the cement matrix increases due to the irregular surface texture of EPSBs and complex packing arrangements arising from varied size distributions. Second, the hydrophobic nature of polystyrene surfaces leads to poor wetting with cement paste, necessitating higher SP dosages to overcome surface

Table 2: Chemical composition of ordinary Portland cement (OPC) Type 1 42.5 R used [32] by XRF analysis and its Bogue potentials [33].

Constituent	CaO	SiO_2	MgO	Al_2O_3	SO_3	Fe_2O_3	K_2O	Na_2O	Loss on ignition
Percentage (%)	62.93	22.36	1.4	5.05	2.61	3.71	0.52	0.15	1.37
Bogue potentials									
Reactant	Tricalcium silicate (C_3S)		Dicalcium silicate (C_2S)		Tricalcium aluminate (C_3A)		Tetra calcium alumino ferrite (C_4AF)		
Percentage (%)	45.62		26.24		8.22		8.83		

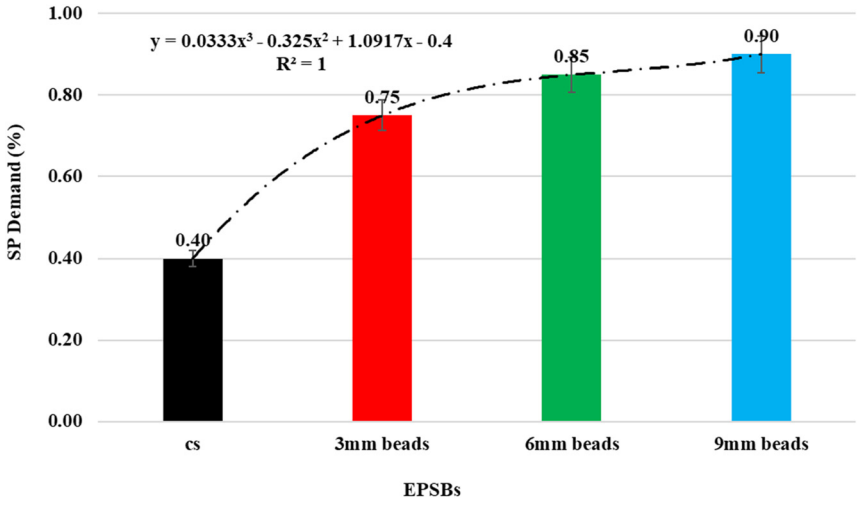

Figure 2: SP demand of samples as per varying sizes of EPSBs.

tension, improve dispersion of the hydrophobic inclusions, and prevent EPSBs agglomeration. Third, the shape factor plays a role as larger EPSBs tend to deviate more from spherical geometry, leading to increased inter-particle interlocking, elevated flow resistance during mixing, and consequently higher SP demand to achieve the required flowability. Statistical analysis supports these findings, with a coefficient of variation ranging between 2.8 % and 4.2 %, and a statistically significant effect of EPSBs size on SP demand confirmed by ANOVA ($p < 0.001$). A strong correlation ($R^2 = 1.00$) was observed between EPSBs size and SP requirement (Figure 2).

3.3 Flow of SCMO

Figure 3 shows the flow times of controlled and energy-efficient SCMO, measured using the standard Hagerman's mini slump cone. The cone used conforms to the size of $(6 \times 7 \times 10)$ cm^3 as suggested by Rizwan et al. [25]. Two marks of 25 cm and 30 cm diameters were placed on the glass plate, and these times are a function of plastic viscosity and the yield stress. Figure 3 shows the T25 cm and T30 ± 1 cm flow times of various studied formulations. The test results reported represent average of three tested readings.

T25 cm time and T30 cm time tests are relative rheological indices of plastic viscosity and yield stress of a cementitious system. As the size of EPSBs in SCMO increases, the flow time increases (Figure 3). The formulation S10 with 0.2 % of 9 mm EPSBs showed the highest delay in flow time for both times as compared to the CS, probably due to higher internal friction and friction at the interface. The lower value of R^2 for plastic viscosity shows its sensitivity towards EPSBs size and its percent content. High internal friction has to be overcome during flow, requiring high SP dosages. From the above results, the T25 cm flow time is dominantly indicative of plastic viscosity [34], and it marginally increased with an increase in EPSBs size. However, T30 cm flow time is indicative of yield stress, appreciably increased with an increase in EPSBs size. Initial setting times increased with an increase in EPSBs size. However, for a given bead size, the final setting time remained almost similar, with larger beads giving increased flow time.

T25 cm and T30 ± 1 cm flow times are qualitative rheological indices. The authors developed a novel quantitative approach later [35].

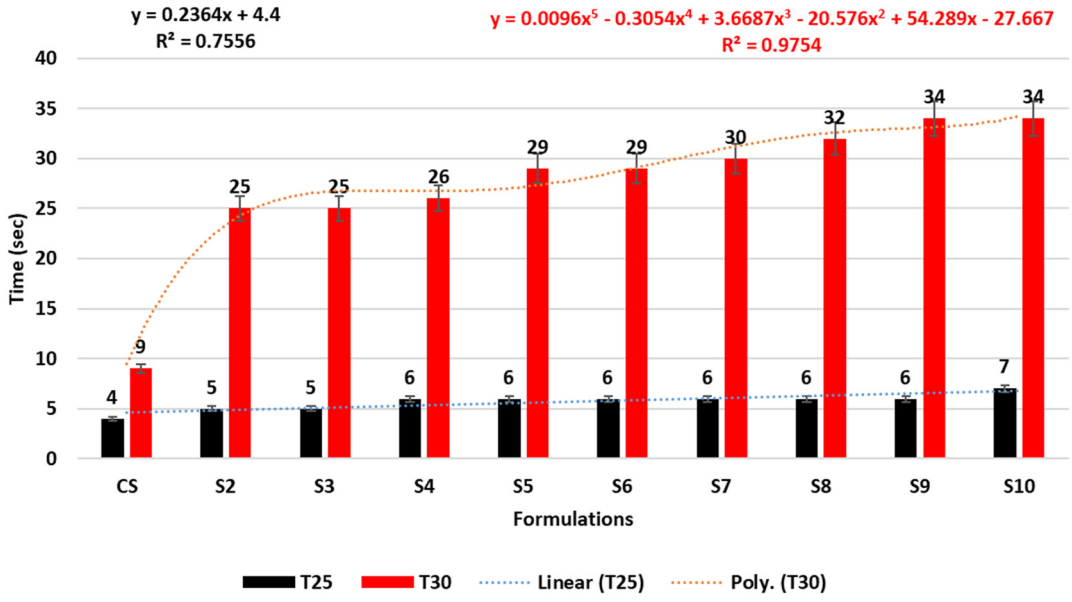

Figure 3: Comparison of T25 cm and T30 cm flow time of SCMO samples having target flow with variable size and contents of EPSBs.

3.3.1 Rheological analysis using bingham model

Rheological behavior of the SCMO formulations was characterized using the Bingham model, converting flow time data into yield stress and plastic viscosity parameters as per the method by Ferraris & de Larrard (1998) [36]. The yield stress (τ_0) and plastic viscosity (μ_p) were calculated based on material density, flow cone geometry, and flow times at defined diameters. Results showed a progressive increase in both yield stress and plastic viscosity with EPSBs size: from 12.5 ± 1.2 Pa and 8.4 ± 0.8 Pa s in the control mix (CS) to 31.2 ± 2.8 Pa and 21.4 ± 1.9 Pa s in the S10 formulation. According to EFNARC classification, all mixes remained within acceptable rheological limits for self-compacting mortars, transitioning from SF (slump flow) to VF (viscous flow) categories with increasing EPSBs size. This rheological shift highlights the importance of selecting mix formulations based on specific placement conditions to ensure adequate flow and workability in practical applications.

3.4 Setting times of SCMO

Figure 4 shows the Vicat [29] setting times of 10 formulations used in this research for energy saving estimation. Setting times for energy-efficient samples and the control SCMO samples were estimated according to BS-EN 196–3 [28]. The test results reported represent average of three tested readings.

The use of EPSBs in SCMO in the presence of ANG powder stabilizes the systems and makes them internally cured as well [24]. The initial and final setting times are lowest for the CS as compared to the samples containing EPSBs and ANG powder, showing a maximum delay of 93 and 210 min (sample S10) in the initial and final setting times of the SCMO, respectively, compared to the CS (Figure 4). It was also observed that for all the samples with the same size EPSBs, there was a constant trend for an increase in initial and final setting times.

The observed setting time delay in SCMO can be attributed to combined effects of ANG and EPSBs. Acacia Nilotica Gum (ANG) retards hydration through calcium ion complexation via its carboxyl and hydroxyl groups, which temporarily reduce the availability of Ca^{2+} for C_3S and C_3A reactions. Additionally, ANG adsorbs onto cement particle surfaces, forming a diffusion barrier that slows water access, while also increasing pore solution viscosity, thereby limiting ion mobility and delaying key hydration processes. EPSBs further contribute to the delay by reducing heat dissipation during hydration, physically obstructing ionic transport, and slightly modifying local water availability through surface moisture interaction. Calorimetric analysis confirms a progressive delay in rate of hydration and peak heat evolution with an increase in EPSBs sizes, mirroring the setting time trends and reinforcing that the primary mechanism is rooted in hydration kinetics modulation.

3.5 Compressive strengths of SCMO

Figure 5 shows the compressive strength of SCMO at three distinct ages (1, 14, and 28 days) by taking average of three

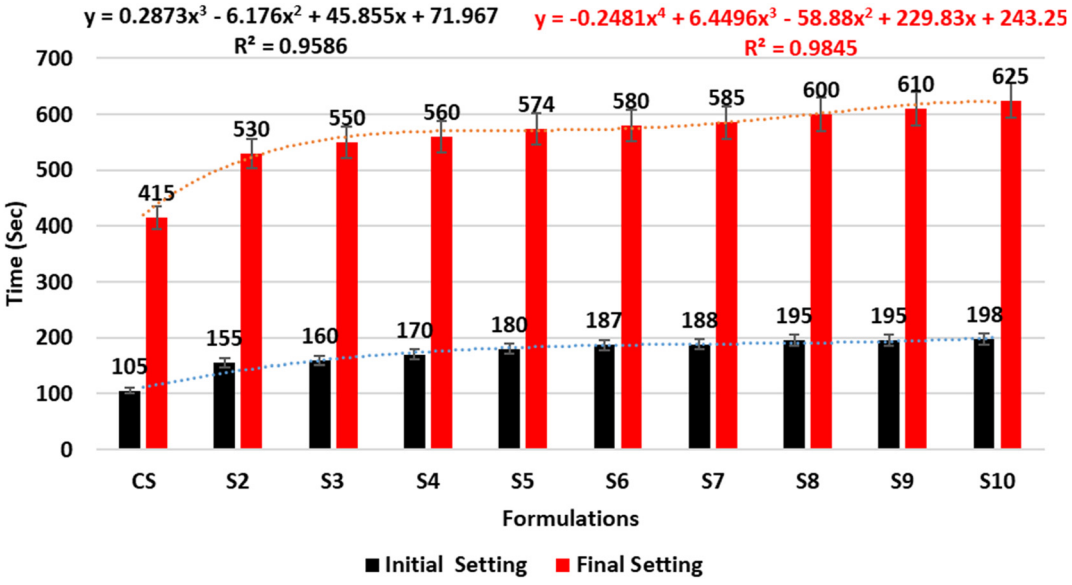

Figure 4: Setting time of SCMO samples with respect to different content and size of EPSBs.

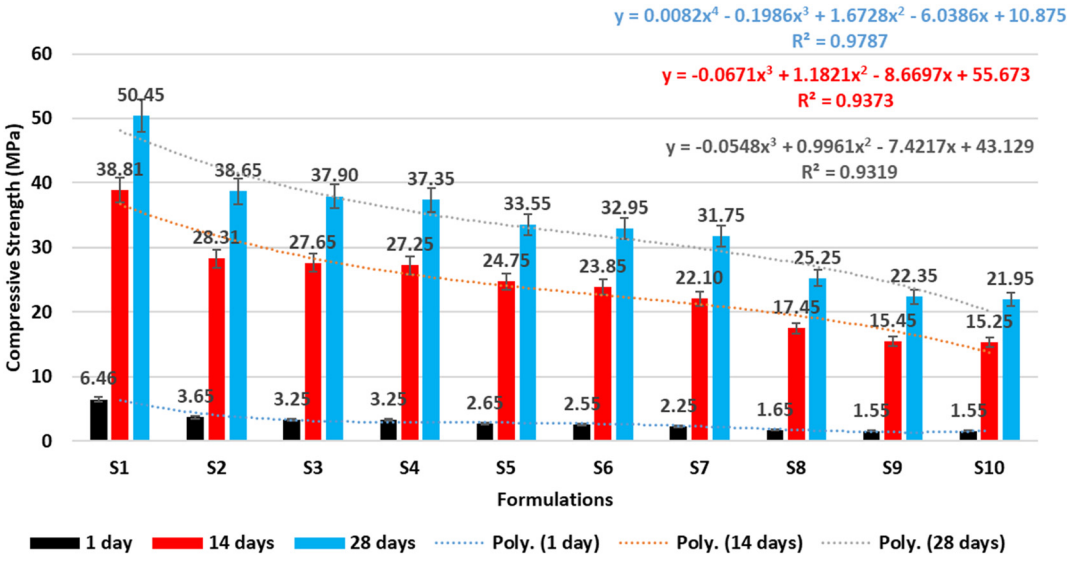

Figure 5: Development of compressive strength of SCMO formulations with respect to age, different contents and size of EPSBs.

identical specimens. The compression test was performed in a compression testing machine at a loading rate of 2.4 kN/s until the fractures appeared.

Compressive strength at 14 and 28 days decreases with an increase in EPSBs sizes, with respect to the CS, which is due to increased porosity and lighter weight of EPSBs acting as a kind of void. The water absorption in SSD conditions for SCMO increased with time. This may be due to higher pore sizes having possibly connected porosity with the increase in EPSBs sizes. The compressive strength of SCMO continued to decrease with the introduction of EPSBs in the mixture. A similar trend of decreasing compressive strength by the addition of EPSBs was observed by Ning Liu et al. in their study [37]. The compressive strength in this research for the CS at 28 days was 50.5 MPa, whereas it reduced to 37.4 MPa for 0.2 % of 3 mm beads SCMO (Figure 5, sample S4). With the increase in size of EPSBs to 6 and 9 mm with a 0.2 % content, the compressive strength was further reduced to 31.8 MPa and 21.9 MPa, respectively (Figure 5, samples S7 and S10). This is due to the presence of EPSBs in SCMO, which possibly act like engineered air voids, because EPSBs contain approximately 98 % air within themselves.

The strength-to-density ratios and efficiency indices further quantify this trend, with normalized strength decreasing from 1.00 in the control (CS) to 0.43 in S10. Efficiency indices, which account for both structural and thermal performance, followed a similar pattern. The strength reduction was also size-dependent, with an estimated loss of 13.1 MPa, 18.7 MPa, and 28.6 MPa per 0.1 % EPSBs size of 3 mm, 6 mm, and 9 mm, respectively. Despite these reductions, all mixes except S10 surpassed the minimum compressive strength requirement of 17–21 MPa outlined by ACI 546.3 R for structural repair mortars, confirming their suitability for overlay applications under moderate loading conditions while offering improved thermal performance.

The strength reduction with EPSBs inclusion can be attributed to several mechanisms: (1) EPSBs-matrix interface weakness due to the hydrophobic nature of polystyrene surfaces, which creates poor bonding with the hydrophilic cement matrix; (2) increased porosity and void content as EPSBs act as lightweight inclusions; and (3) stress concentration effects around EPSBs under loading. Literature indicates that EPSBs-cement interfaces typically exhibit weak bonding due to the non-polar nature of polystyrene, which cannot form chemical bonds with cement hydration products. The 98 % air content within EPSBs effectively creates engineered voids that reduce the load-bearing cross-sectional area of the matrix.

3.6 Water absorption of SCMO

Figure 6 shows the water absorption for SCMO at two different ages, namely 14 days and 28 days showing the discontinuity of pore networks, if any, and indirect pore refinement. Water absorption was calculated by the conventional method by taking average of three identical specimens.

Water absorption of the SCMO increased by adding EPSBs and ANG powder. With an increase in EPSBs size, the water absorption increased by a maximum of 23.4 % for 14 days and 31.4 % for 28 days, with respect to water absorption in the CS. It was also observed that for all the samples with the same EPSBs size, there was a constant trend of increase in water absorption from 14 to 28 days. Also, since EPSBs are non-absorbent of water, this increase of water absorption (water uptake) may be due to the presence of air or internal porosity. ANG powder might have created voids while acting as a kind of internal curing agent in the SCMO with increased hydration. Nadhim Hamah et al. [38] also found the increasing water absorption as the number of EPSBs replaced increased.

Water absorption results, shown in Figure 6, demonstrate a clear increase with EPSBs size, rising from 1.91 ± 0.10 % in the control mix (CS) to 2.51 ± 0.12 % in S10, an 31 % increase. This trend is attributed to microstructural changes induced by both the EPSBs inclusion and the ANG-modified matrix. Poor bonding at the hydrophobic EPSBs surfaces leads to interfacial transition zones (ITZs), which serve as preferential pathways for water ingress. Larger EPSBs generate more extensive ITZ networks, enhancing water absorption. Simultaneously, ANG's hygroscopic nature introduces microscopic water retention sites that evolve into accessible capillary pores during drying, further contributing to absorption. The stepwise increase in absorption across formulations S4, S7, and S10 indicates a progressive development of pore

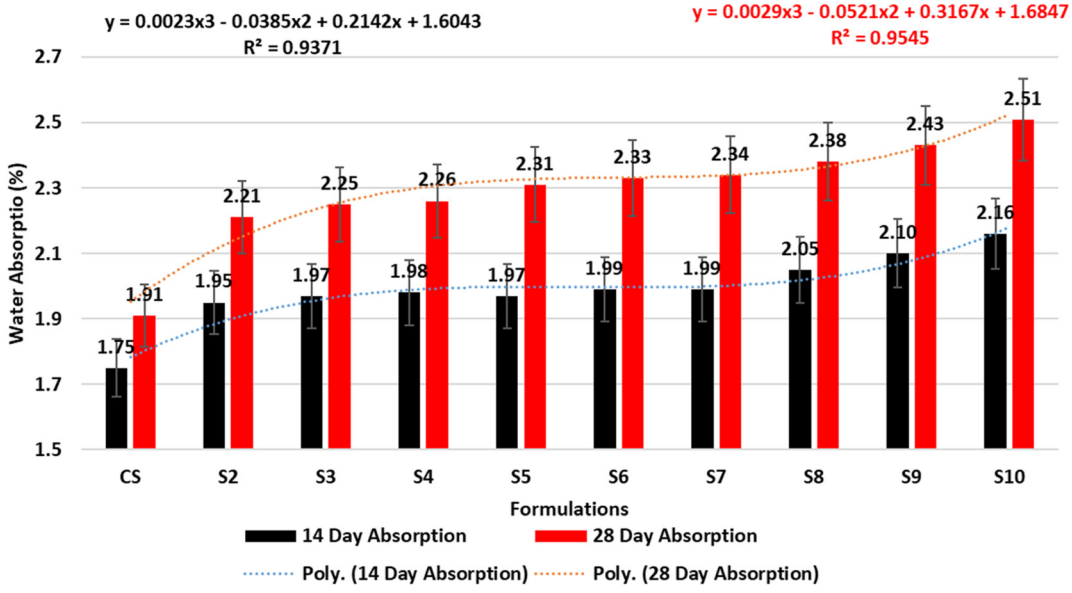

Figure 6: Water absorption of SCMO samples with respect to age, different contents, and sizes of EPSBs.

connectivity. Notably, this enhanced pore network correlates with improved thermal insulation, as the formulations with the highest absorption also exhibited the lowest thermal conductivity. This suggests that the microstructural features responsible for increased water uptake also facilitate thermal resistance, linking porosity evolution to multifunctional performance in EPSBs-modified SCMO.

3.7 Early linear shrinkage of SCMO

Early shrinkage measurements were performed on SCMO and are shown in Figure 7 for first 24 h using the modified German Schwindrinne apparatus with (4 × 6 × 25) cm^3 channels. The test results reported represent average of three identical specimens. Maximum 24 h shrinkage was observed for the control mix, as anticipated, and reduced shrinkage was observed with an increase in EPSBs size. This reduction in shrinkage may be attributed to increased porosity, which possibly acts as a cushion for accommodating shrinkage strains. The shrinkage looks to be predominantly chemical shrinkage during the first 24 h [39]. The ASTM prescribed measurement of drying shrinkage using a dilatometer after 24 h certainly misses this early age shrinkage, which is quite important [40, 41].

This trend is linked to several mechanisms: EPSBs serve as internal cushioning zones that dissipate shrinkage-induced stresses; their inclusion also increases porosity, providing void space for strain accommodation; and the reduced hydration efficiency associated with EPSBs limits overall shrinkage potential. These factors collectively result in a longer early expansion period and significantly lower shrinkage rates. From a practical perspective, this behavior is advantageous for overlay applications by minimizing early-age cracking, enhancing dimensional stability, and improving substrate adhesion. Although long-term shrinkage testing per ASTM C157 is pending, the observed early-age trends suggest a potential 20–40 % reduction in 28-day drying shrinkage, offering promising implications for durable overlay systems.

3.8 Calorimetric response of SCMO

The calorimetry of SCMO was performed on a semi-adiabatic calorimeter FCAL 8100, USA and temperature log details were plotted for 24 h as shown in Figure 8.

When shrinkage and calorimetric responses are seen together, it becomes obvious that the rate of hydration slows down with an increase in EPSBs sizes. Calorimetric studies also showed that the evolution of heat of hydration decreased with the increase in EPSBs content in SCMO formulations, possibly due to increased porosity.

3.9 X-ray diffraction of SCMO

X-ray diffraction analysis was conducted at 60 days to ensure near-complete hydration and stable crystalline phase development (Figure 9). This analysis helps understand how EPSBs incorporation affects cement hydration products, which directly influences the thermal conductivity and mechanical properties reported in previous sections. The crystalline phases present affect heat transfer pathways and matrix bonding characteristics. XRD results provides acceptable information about the most probable phases and is considered as a sensitive technique [42].

The peaks and classification show the prominent crystalline hydration products. From the XRD analysis of the CS, it may be seen that the dominant crystalline peaks included albite, grossite, portlandite, quartz, and calcite and were the major crystalline hydration products. Whereas Figure 10 shows the diffractogram obtained when the EPSBs, ANG and SP are within a typical SCMO formulation. Very low Portlandite (CH) occurs at 2θ values of around 18 and 34°. This

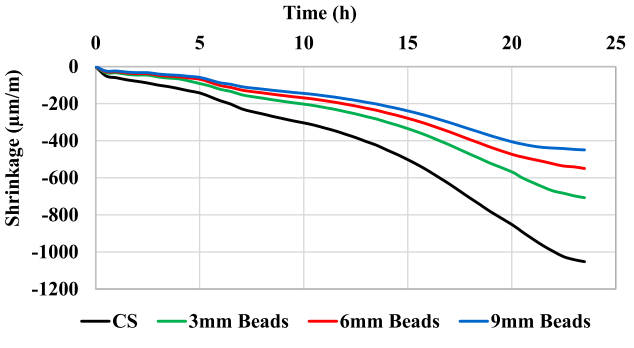

Figure 7: Comparison of the early 24 h shrinkage of SCMO having different sizes of EPSBs 0.2 % content.

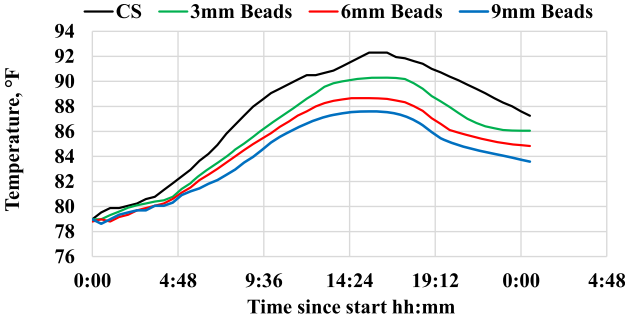

Figure 8: Calorimetric response of SCMO having different sizes of EPSBs of 0.2 % content. Note: 1 °F (degree fahrenheit) is −17.222 °C (degree celsius).

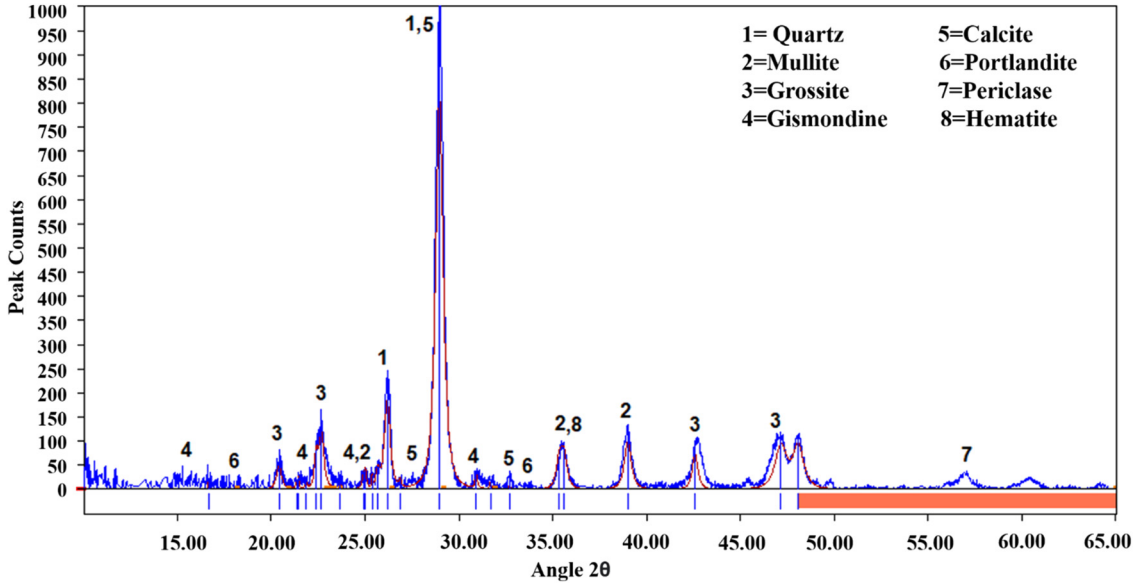

Figure 9: X-ray diffractogram of control sample.

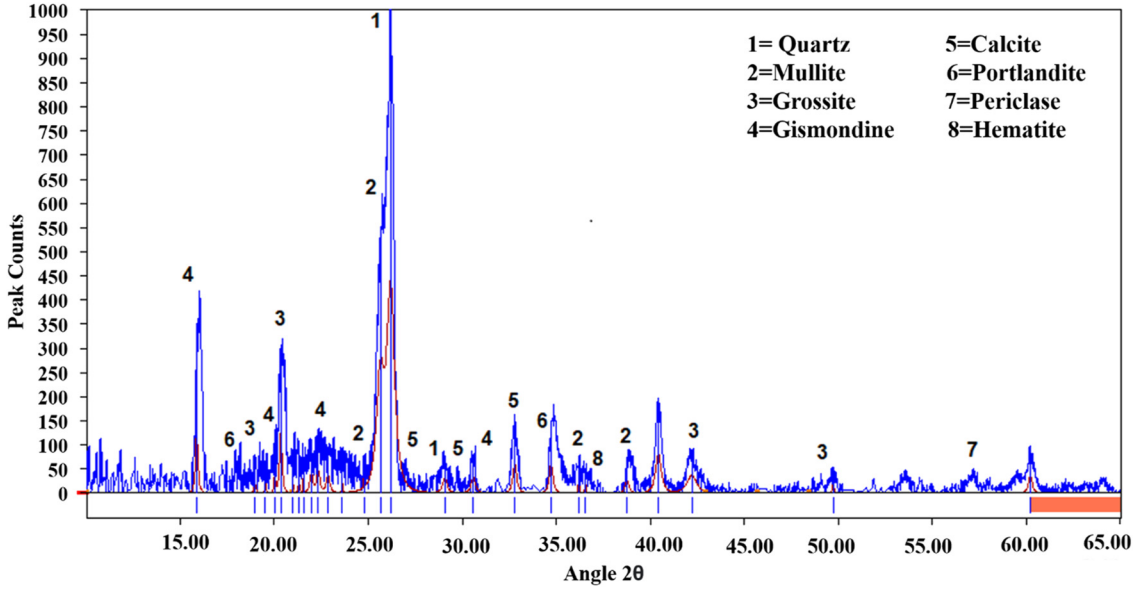

Figure 10: X-ray diffractogram of self-compacting energy-efficient SCMO with 6 mm EPSBs size of 0.2 % content.

means that in the presence of EPSBs, the mullite, grossite, gismondine, quartz, calcite, and portlandite are significant.

3.10 Thermal conductivity of control and other SCMO with EPSBs

Thermal conductivity response was measured according to ASTM C518 on a sample of $(50 \times 50 \times 50)$ mm^3. Figure 11 shows the thermal conductivity response based on the EPSBs size. The test results reported represent average of three identical specimens.

The use of EPSBs has been found to render SCMO energy-efficient and make them sustainable solutions. The EPSBs provide a reasonable reduction in the thermal conductivity of the SCMO. As shown in Figure 11, thermal conductivity decreased from 0.1589 to 0.0615 W/m.K when EPSBs of different sizes were introduced in the mixture of SCMO. According to energy analysis, this decreased the thermal conductivity values with the inclusion of insulating EPSBs in

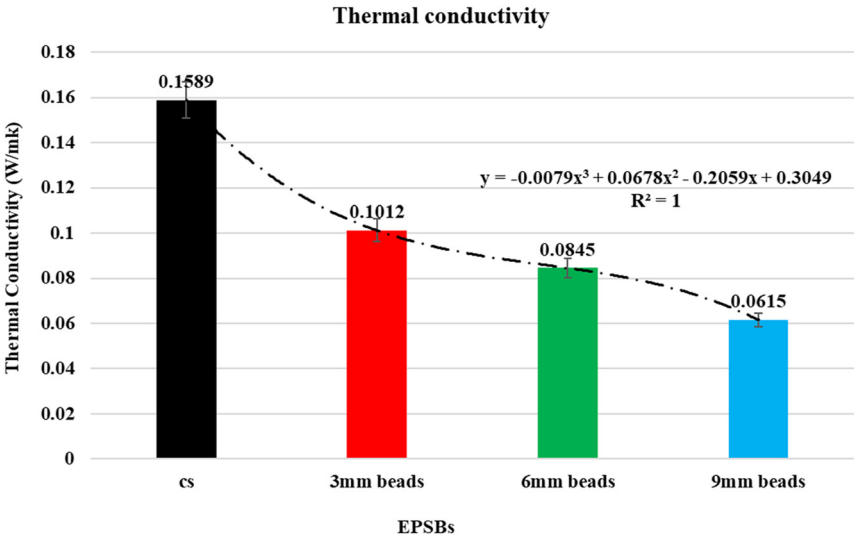

Figure 11: Comparison of thermal conductivity response between control and SCMO containing different sizes of EPSBs of 0.2 % content.

SCMO. Another reason may be the presence of the ANG powder which creates internal water entrainment. Conductive heat transfer through SCMO using EPSBs was measured using the Fourier's Law (Equation (1)) [43].

$$q = (k/s)\,A\,dT\ (W, Btu/h) \tag{1}$$

The heat transfer per unit area is given by equation (2).

$$q/A = (k/s)\,dT\left(W/m^2, Btu/\left(h\,ft^2\right)\right) \tag{2}$$

Where,

k = Thermal conductivity of material (W/m.K or W/m.C, Btu/(h ft °F))

s = Material thickness (m, ft).

A = Heat transfer area (m^2, ft^2).

dT = t_1-t_2 = temperature gradient across the material (^{0}C/K).

In this study, it was considered that heat transfers through 0.0381 m (1.5 inch or 4 cm) thick layer of SCMO. The K values were determined earlier for control SCMO sample and EPSBs modified SCMO mortars with three sizes of polystyrene bead (3, 6, and 9 mm) as per ASTM C518. The typical temperature on the outer side of the SCM overlayed wall was assumed to be 42 °C and 25 °C on the indoor side, as per the local conditions in the summer season with a temperature difference of 17 °C (62.6 K). Figure 12 shows the conductive heat transfer through a 0.0381 m thick SCM overlayed wall of 1.0 m^2 area with temperature difference of 17 °C (62.6 K), whereas the thermal conductivity for each sample type is given in Figure 11.

Figure 12 shows that the maximum heat per unit area transferred by the control SCMO sample was 97.9 W/m^2 for temperature difference of 17 °C across the two sides of SCMO whereas heat transfer through SCMO using 3, 6, and 9 mm EPSBs was 62.35, 52.06, and 37.89 W/m^2, respectively, for the same temperature difference of 17 °C (the margin of error was less than 5 %). It is clear that the use of SCMO using EPSBs topping reduces energy consumption by 36.3 %, 46.8 %, 61.3 % for 3, 6, and 9 mm EPSBs, respectively, thus demonstrating an energy-efficient solution in buildings. Earlier, it was shown in a side investigation that [44] EPSBs of 6 mm size gave the optimized response in both fresh and hardened states. The present investigation also seems to supplement the earlier results.

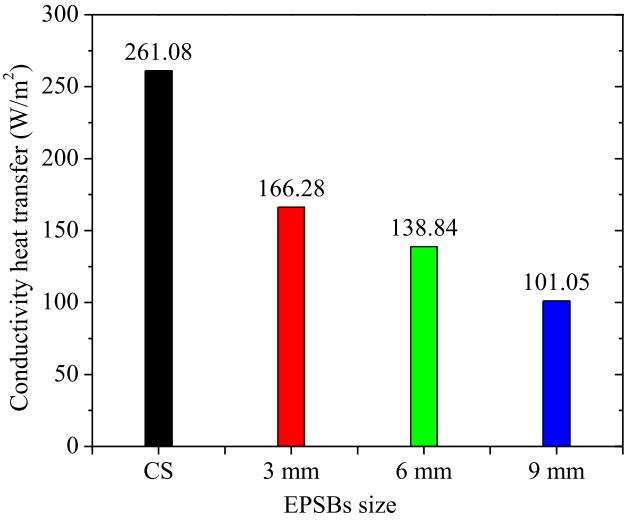

Figure 12: Comparison of conductivity heat transfer between control and SCMO having EPSBs of 0.2 % content.

3.11 Scanning Electron Microscopy of SCMO with EPSBs

Figure 13 shows an SEM image of the S6 SCMO formulation incorporating 6 mm diameter EPSBs with 0.15 % content.

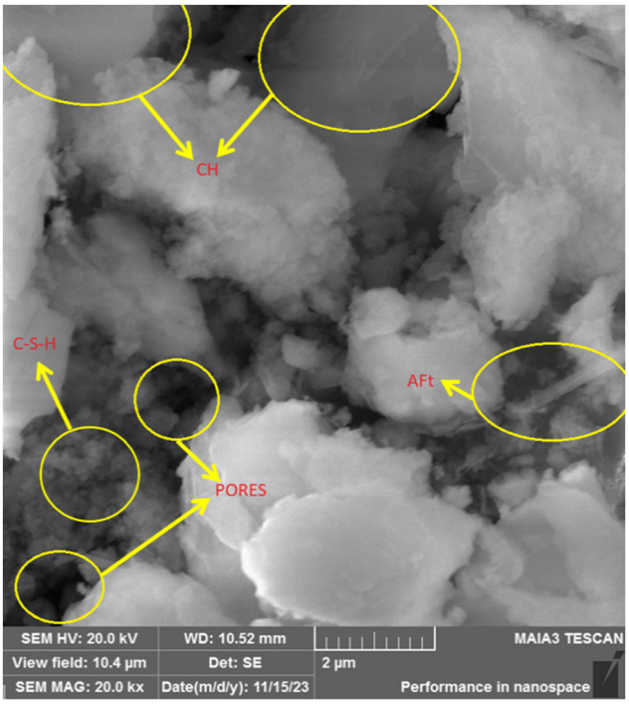

Figure 13: Scanning electron microscope image of SCMO formulation S6 using EPSBs.

Due to the presence of EPSBs, porosity of the structure has been seen in the SCMO formulation. Hydration products like CSH gel, ettringites can also be seen in Figure 13.

3.12 BET-nitrogen sorptivity of SCMO with EPSBs

V-Sorb 2800 P surface area and porosimetry was used for SCMO S6 formulation to look at qualitative analysis of pore structure in the matrix. This size was investigated because the earlier study [44] had shown that this size of EPSBs gave the optimized response in both the fresh and hardened state properties of SCMO formulations incorporating EPSBs. It is shown that with the incorporation of EPSBs, the porosity of SCMO formulations increases. Figure 14 shows BET nitrogen adsorption and desorption curves. The hysteresis phenomenon, especially between relative pressures of 0.6–0.9 indicates that the system has a porous structure. Beyond relative pressure of 0.9, up to 1, significant gas adsorption and desorption take place, indicating a connected porosity.

The results shown in Figures 14 and 13 are in agreement and support the properties of SCMO formulations investigated

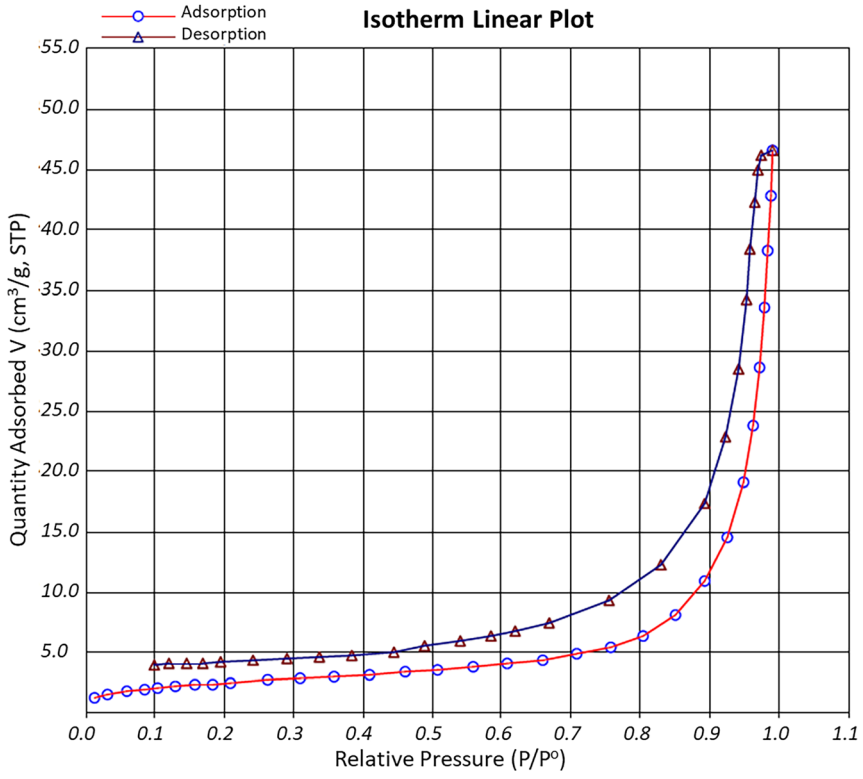

Figure 14: BET-nitrogen porosimetry of the SCMO formulation S6 with EPSBs.

in fresh and hardened states. The specific surface area = 8.61 m^2/g, volume of pores was 0.073002 cm^3/g, and porosity was 30.62 %.

4 Conclusions

The results show that EPSBs size and content play a crucial role in defining the fresh and hardened characteristics of SCMO. Because EPSBs are light, it becomes difficult to get them uniformly suspended in the SCMO matrix. Therefore, a polycarboxylate-ether-based SP, along with ANG powder (acting as viscosity-enhancing agent), was used to overcome this issue with minimal influence on fresh and hardened properties of the formulations investigated. Important findings of this study are summarized as follows:

1) SP demand increased with the increase in the size of EPSBs. The SP demand in terms of binder weight increased from 0.75 to 0.85 and 0.85 to 0.90 with an increase in size of EPSBs from 3 mm to 6 mm and 6 mm–9 mm, respectively, which is mostly due to internal frictions as they are water repellent but allow air to pass through.
2) With the increase of EPSBs size, the flow and setting times increased, having adverse effects on compressive strength. The 28-day compressive strength of SCMO having 0.2 % of 3 mm beads was observed as 37.4 MPa, which is 26 % less than that of CS (50.5 MPa). With the increase in size of EPSBs to 6 and 9 mm with a 0.2 % ratio, the compressive strength was further reduced by 37 % (31.8 MPa) and 57 % (21.9 MPa), respectively. However, the strength drop can be minimized by using suitable synergetic supplementary cementitious materials, as has been demonstrated by the authors in previous studies [44, 45].
3) The CS demonstrated a maximum 24 h shrinkage and a significant reduction of shrinkage observed with increasing size of EPSBs incorporated in SCMO formulations w.r.t the CS. This reduction in shrinkage may be attributed to increased porosity, which possibly acts as a cushion for accommodating shrinkage strains.
4) The thermal conductivity of SCMO decreased with increasing size and content of EPSBs. The thermal conductivity gradually decreased with increasing size of EPSBs from 0.1589 W/m·K for CS to only 0.0615 W/m.K for EPSBs of size 9 mm, possibly due to reduced surface areas associated with larger sizes.
5) It was evident that the use of SCMO toppings had reduced energy consumption by 36.3 %, 46.8 %, and 61.3 % for EPSBs of size 3, 6, and 9 mm, respectively. Therefore. It may be concluded that the addition of EPSBs results in energy-efficient, sustainable SCMO and possibly concrete, which shows less heat transfer as compared to conventionally used mortar and concrete systems. Such energy-efficient SCMO can be overlaid suitably on structural elements to increase room comfort.

While this study demonstrates the thermal and mechanical properties of EPSBs-modified SCMO, several important aspects require future investigation for practical overlay applications:

1) Bond strength testing: Pull-off or shear bond tests according to ASTM C1583 are essential to evaluate adhesion between SCMO and concrete substrates.
2) Durability assessment: Long-term performance under freeze-thaw cycles, UV exposure, and weathering conditions needs evaluation for exterior applications.
3) Layer thickness optimization: Systematic study of overlay thickness (10–50 mm) versus thermal performance to determine optimal application parameters.

These investigations will be addressed in future phases of this research program.

Acknowledgments: The authors acknowledge the Deanship of Scientific Research, Vice Presidency for Graduate Studies and Scientific Research, King Faisal University, Saudi Arabia (Grant No. KFU253938). The Authors would like to thank Dr. Konrad Wütz and his colleagues from Master Builders Solutions, Tröstberg, Germany, for providing the chemical admixtures by air, free of charge, used in this research and all previous research by the authors. We are also grateful to the Rector NUCES (National University of Computer and Emerging Sciences), Dr. Aftab Ahmad Maroof and the Sectary General, Rana Ghulam Shabbir SI, of FAST (Foundation for Advancement of Sciences and Technology) for their interest in providing funds for establishing Advanced Materials Laboratory and the financial help granted to the student for supporting this research.

Funding information: This work was supported by the Deanship of Scientific Research, Vice Presidency for Graduate Studies and Scientific Research, King Faisal University, Saudi Arabia [Grant No. KFU253938]. Thanks are also due to the NUCES-FAST Lahore, Pakistan, and NUST Islamabad, Pakistan, for supporting the research.

Author contributions: Syed Ali Rizwan: conceptualization, supervision, investigation, validation, writing, reviewing, and editing; Muhammad Nasir Amin: resources, project administration, investigation, validation, funding acquisition, writing, reviewing, and editing; Hafiz Sajid Ali:

methodology, data acquisition, writing-original draft; Hamza Ali: investigation, writing, reviewing, and editing; Muhammad Tahir Qadir: resources, investigation, funding acquisition, validation, writing, reviewing, and editing; Muhammad Imran: validation, writing, reviewing, and editing. All authors have accepted responsibility for the entire content of this manuscript and approved its submission.

Conflict of interest: The authors state no conflict of interest.

Data availability statement: All data generated or analysed during this study are included in this published article.

References

1. Yang J, Chan K, Venkatesan H, Kim E, Adegun MH, Lee J, et al. Superinsulating BNNS/PVA composite aerogels with high solar reflectance for energy-efficient buildings. Nano-Micro Lett 2022;14:54.
2. Torres M, Lombard LP, Coronel JF, Maestre IR, Yan D. A review on buildings energy information: trends, end-uses, fuels and drivers. Energy Rep 2022;8:626–37.
3. Rodgers L. Climate change: the massive CO_2 emitter you may not know about. BBC News 17 December 2018. https://www.bbc.com/news/science-environment-46455844.
4. Tanuj V, Khitoliya DR, Singh AJ. An evaluative study on energy efficient building materials. Int J Innov Res Adv Eng (IJIRAE) 2016;3:98–103.
5. Shen X, Kim J-K. 3D graphene and boron nitride structures for nanocomposites with tailored thermal conductivities: recent advances and perspectives. Funct Compos Struct 2020;2:022001.
6. Yüksek I. An evaluation of building materials in terms of energy efficiency. Period Polytech Civ Eng 2015;59:45–58.
7. Rizwan SA, Ahmad S, Bier TA. Application of packing concepts to high performance self-consolidating mortar (SCM) systems. USA: ACI Special Publication; 2012, 289:1–17 pp.
8. Gupta N, Siddique R, Belarbi R. Sustainable and greener self-compacting concrete incorporating industrial by-products: a review. J Clean Prod 2021;284:124803.
9. Rizwan SA, Khan H, Bier TA, Adnan F. Use of effective Micro-organisms (EM) technology and self-compacting concrete (SCC) technology improved the response of cementitious systems. Constr Build Mater 2017;152:642–50.
10. Chen B, Liu J. Mechanical properties of polymer-modified concretes containing expanded polystyrene beads. Constr Build Mater 2007;21:7–11.
11. Shabbar R, Al-Tameemi AA, Alhassani AMJ. The effect of expanded polystyrene beads (EPS) on the physical and mechanical properties of aerated concrete. Open Eng 2022;12:424–30.
12. Hu F, Wu S, Sun Y. Hollow-structured materials for thermal insulation. Adv Mater 2019;31:1801001.
13. Herihiri O, Guettala A, Benabed B. An investigation on the physical, mechanical and thermal properties of dune sand mortars lightened by expanded polystyrene beads (EPS). J Silic Based Compos Mater 2021;1:28–36.
14. Sabaa B, Ravindrarajah RS. Engineering properties of lightweight concrete containing crushed expanded polystyrene waste. In: Proceedings of the symposium on Advances in Materials for cementitious composites, December 11–13, 1997. Boston, MA, USA: Materials Research Society; 1997.
15. Hilal N, Sor NH, Faraj RH. Development of eco-efficient lightweight self-compacting concrete with high volume of recycled EPS waste materials. Environ Sci Pollut Control Ser 2021;28:50028–51.
16. Babu D, Babu KG, Weea TH. Properties of lightweight expanded polystyrene aggregate concretes containing fly ash. Cement Concr Res 2005;35:1218–23.
17. Melit L, Calotă R, Amăreanu M, Silica aerogel-incorporated cement and lime plasters for building insulation: an experimental study, Buildings 2024;14:1-12.
18. Gu X, Ling Y. Research progress of aerogel materials in the field of construction. Alex Eng J 2024;91:620–31.
19. Simpson A, Rattigan I, Kalavsky E, Parr G. Thermal conductivity and conditioning of grey expanded polystyrene foams. Cell Polym 2020;39:238–62.
20. Erünal E. Comparison of thermal insulation performance of foam extruded Black EPS. Polym Bull 2024;81:16595–605.
21. Huang Y, Stonehouse A, Abeykoon C. Encapsulation methods for phase change materials – a critical review. Int J Heat Mass Tran 2023;200:620–31.
22. Aftab W, Huang X, Wu W, Liang Z, Mahmood A, Zou R. Nanoconfined phase change materials for thermal energy applications. Energy Environ Sci 2018;11:1392–424.
23. Rizwan SA, Latif W, Bier TA. Response of self-consolidating cement paste systems containing Acacia nilotica gum as an organic admixture. Constr Build Mater 2016;126:768–76.
24. Rizwan SA, Neha Mahmood UM, Bier TA. Response of self-compacting paste (SCP) systems containing Acacia modesta gum. Constr Build Mater 2018;161:398–406.
25. Rizwan SA, Gul S, Bier TA. Self-consolidating paste systems containing Acacia nilotica gum powder. ACI Mater J 2019;116:5–15.
26. Tomori MA, Adedeji AA. Assessment of early compressive strength of self-compacting concrete using different grades of ordinary Portland cement. Webs Journal of Science and Engineering Application 2015;4:252–68.
27. SCC 028. The European guidelines for self-compacting concrete. BIBM, CEMBUREAU, ERMCO, EFCA, and EFNARC; May 2005.
28. BS EN 196-3. A method of testing cement. Part 3: determination of setting times and soundness. UK: BSI; 1995.
29. BS EN 196-1. Method of determining compressive and flexural strength of cement mortar. UK: BSI; 2005.
30. Aalmusallam A. Effect of environmental conditions on the properties of fresh and hardened concrete. Cement Concr Compos 2001;23:353–61.
31. Bergström SG. Curing temperature, age and strength of concrete. Magazine of Confrence Research 1953;5:61–6.
32. Tuaum A, Haileselassie B, Tsehaye Y. Experimental investigation of rigid concrete pavements incorporated with waste lathe scrap steel fiber. In: 1st International conference on Engineering and Technology, Ethiopia: Research Gate; 2020:124–35 pp.
33. Marchment T, Sanjayan JG, Nematollahi B, Xia M. Interlayer strength of 3D printed concrete. In: Sanjayan J, Nazari A, Nematollahi B, editors. 3D concrete printing technology. Oxford, UK: Elsevier; 2019: 241–64 pp. ISBN 9780128154816.
34. Rizwan SA. High-performance mortars and concrete using secondary raw materials [Ph.D thesis]. Germany: Technical University Freiberg; 2006. 161 pp.

35. Mahmood U, Bier T, Rizwan S. Assessing rheology of self-compacting paste systems—A new approach. ACI Mater J;118:2021.
36. Ferraris FC, de Larrard F. Testing and modelling of fresh concrete rheology, NISTIR 6094, February 1998. SCIRP Open Access March 2011;3.
37. Liu N, Chen B. Experimental study of the influence of EPS particle size on the mechanical properties of EPS lightweight concrete. Constr Build Mater 2014;68:227–32.
38. Sora NH, Hilal N, Faraj RH, Ahmed HU, Sherwani AFH. Experimental and empirical evaluation of strength for sustainable lightweight self-compacting concrete by recycling high volume of industrial waste materials. Eur J Environ Civ Eng 2021:1–18.
39. Kheir J, Hilloulin B, Loukili A, Belie ND. Chemical shrinkage of low water to cement (w/c) ratio CEM I and CEM III cement pastes incorporating silica fume and filler. Materials 2021;14:1164.
40. Lura P. Autogenous strain of cement pastes with superabsorbent polymers. In: International RILEM conference on volume changes of hardening concrete: testing and mitigation. Denmark: Lyngby DTU; 2006:57–65 pp.
41. Elyamany HE, Elmoaty AEMA, Mohamed B. Effect of filler types on physical, mechanical and microstructure of self-compacting concrete and flowable concrete. Alex Eng J 2014;53:295–307.
42. Sharaf F. The impact of thermal mass on building energy consumption: a case study in Al Mafraq city in Jordan. Cogent Eng 2020;7:1–18.
43. Ali HS. Study of energy efficient SCM systems. [M.Sc. thesis]. Lahore: NUCES-FAST; 2021:1–75 pp.
44. Faheem A, Rizwan SA, Beir TA. Properties of self-compacting mortars using blends of limestone powder, fly ash, and zeolite powder. J Constr Build Mater 2021;286:122788.
45. Rizwan SA, Beir TA. Blends of limestone powder and fly-ash enhance the response of self-compacting mortars. Constr Build Mater 2012;27: 398–403.